International Conference on Space Optics—ICSO 2018

Chania, Greece

9–12 October 2018

Edited by Zoran Sodnik, Nikos Karafolas, and Bruno Cugny

Improved low dark current MWIR/LWIR MCT detectors: first results of ROIC and MCT tests

Holger Höhnemann

Stefan Hanna

Ajit Kumar Kalgi

Dirk Van Aken

et al.

International Conference on Space Optics — ICSO 2018, edited by Zoran Sodnik, Nikos Karafolas, Bruno Cugny, Proc. of SPIE Vol. 11180, 111806G · © 2018 ESA and CNES · CCC code: 0277-786X/18/$18 · doi: 10.1117/12.2536151

Improved Low Dark Current MWIR/LWIR MCT detectors: first results of ROIC and MCT tests

Holger Höhnemann
Holger Höhnemann[*a], Stefan Hanna[a], Ajit Kumar Kalgi[b], Dirk van Aken[b], Rashme Sudiwala[c], Peter Hargrave[c], Werner Gross[a]
[a]AIM Infrarot-Module GmbH, Theresienstraße 2, 74072 Heilbronn, Germany; [b]Caeleste CVBA, Hendrick Consciencestraat 1b, B2800 Mechelen, Belgique; [c]Cardiff University, School of Physics & Astronomy, 5 The Parade, Cardiff CF24 3AA, United Kingdom

ABSTRACT

Within the TRP program "Development of Low Dark Current MWIR/LWIR Detectors" ne MCT material was tested with reduced dark current for low photon flux applications. A specific ROIC design was set up within this program to allow a proper characterization of the material and act as a demonstrator for further ROIC derivates. Demonstrator assemblies were prepared and tested.

The poster will highlight the specific design approaches for the ROIC and the MCT. Four different topologies for the input stage on the ROIC were implemented to allow direct assessment of the impact of the design approach. A part of these input stages were designed using radiation hardened cell library. The ROIC doesn't contain any internal state machine but id fully controlled via a high speed SPI interface driven by an external sequencer.

A test setup will be highlighted. A liquid helium cryostat was prepared to allow dark current measurements in an environment which does not suffer from parasitic radiation sources. The same setup is capable for operation with external illumination and optical filers, which can be moved into the beam.

The detector assemblies are presented. A two-step approach is shown which is initially scanning the performance of the different input topologies. A final detector assembly is selected upon the best performance; final assemblies are shown, the test results will be given on the poster.

Keywords: MCT, MWIR,LWIR, Dark Current

1. INTRODUCTION

During the last decades AIM has established a fundamental competence for MCT based IR detectors from short wave to very long wave detection range. In the beginning these imaging detectors have been exclusively used in defensive industries, mainly due to classification as military goods and high costs of such devices. In recent years, this wide range of technology was used in space instruments too, with an increasing number of commercial and industrial applications using in the long wave and very long wave infrared spectrum.

To satisfy these needs, AIM has constantly improved the technology for LWIR and VLWIR detectors. AIM has the advantage of having all necessary technologies for manufacturing of high performance MCT sensor modules and cameras under one roof. Large sized CdZnTe substrates are grown in-house. The photo-sensitive MCT-layers are formed by liquid phase epitaxy (LPE) and the PV-chips are subsequently hybridized to AIM-designed silicon readout integrated circuits (ROIC) via Indium bump technology to form focal plane arrays (FPAs). The FPAs are integrated into Dewars and fitted with AIM manufactured Linear Stirling coolers. High performance command and control electronics (CCE) allows digital interfacing and easy control of the so called Integrated Detector Cooler Assemblies (IDCA). The IDCAs are delivered to the customers, who integrate these into their systems for all kind of imaging and hyperspectral imaging applications. As these systems are very diverse, often customer specific modifications, e.g. different cold shield apertures

* holger.hoehnemann@aim-ir.com; phone +49-7131-6212-188; fax +49-7131-6212-199; www.aim-ir.com

(FOVs) and/or the integration of customer specific (cold) filters, are made. Furthermore, AIM does also manufacture fully integrated cameras.

An important advantage of MCT based detectors is the tunable band gap. The spectral sensitivity of MCT detectors can be engineered to extend to cut off values of about 15 µm. The drawback of these devices is the intrinsic leakage current of photo diodes in this detection area, generally called dark current. This dark current is limiting the applicability of the detector for several applications. To overcome this limit, the temperature dependent reduction of the dark current at reduced temperatures is used to operate with low dark currents. Typical operation conditions are around 60K. For further reduced temperatures a saturation level of the dark current was found around 50K and was reported in several publications.
Within the frame of the former ESA TRP program low dark current this level could be reduced to settle the dark current baseline at about 45K. These activities were continued in the frame of the actual program.

2. OBJECTIVES OF THE PROGRAM

The need for astronomy missions is giving two key parameters for the necessary detectors:
First it has to be capable to handle very small photon fluxes down to photon counting. Therefore a detector shall be available having sufficiently small charge handling capacities to be sensitive in the required illumination range. This will also increase the sensitivity and accuracy of the dark current measurements, since in the former programmes available ROICs with high charge capacitances were used. These devices were operated at the lower limit of their detectivity; so much effort has to be taken to ensure the accuracy in this operating region.
To overcome this critical issue a new ROIC was addressed within this program for be a breadboard sample for future astronomy applications. This ROIC shall be used for the analysis of the optimized MCT material.
A further issue was found in the assembly condition. It was found very critical to achieve a required dark condition for the measurement of the dark current. With excessive shielding effort for internal assemblies the base level of the measured dark current could be reduced to the level formerly reported. However, it could not be clearly distinguished if this base level was due to residual illumination or a real impact of the MCT. Therefore a light tight test setup was set up within this program using a LHe based cryostat to ensure the lack of residual photon impact during the dark current measurement.
The third area of optimization was the MCT material itself. Different assumptions on the origin of the base level of the dark current were reviewed. The assumption of recombination centers at the surface of the MCT was found to be the most appropriate one and has been reported in several publications. So the task for AIM was to find process optimizations which will improve the surface conditions and thereby further reduce the base level of the dark current. This optimization was applied to both types for MCT detector diodes: n on p and p on n type.

3. LDC - ROIC

The ROIC design was done by Caeleste BV. It comprises an array size of 1280x1080 pixels. To assess in this study the impact of different input cell designs, this area was divided into four segments with 320x1080 pixels. Each of these segments is providing their data by a separate video output. The basic ROIC specification is given in table 1; Figure 1 is indicating the basic layout of this chip.

Table 1: Basic ROIC characteristics

Item	Video
Input capabilities	N on P and P on N devices
Array size	4x 320x1080 pixel
Input cell topology	7T cell design, Rad hard 5T cell design. Rad hard 5T cell design, standard Source follower
Pixel size	20µm x 20µm
CHC	700 ke- ; 1400 ke-
Pixel readout rate	20 MHz
Shutter modes (external sequencer)	Integrate While Read (IWR) Integrate Then Read (ITR) Rolling shutter (RS) Non-Destructive Readout (NDR) or Fowler sampling
Operating temperature	40K … 80K (nominal)
Technology	CMOS 0,18 µm; XFAB

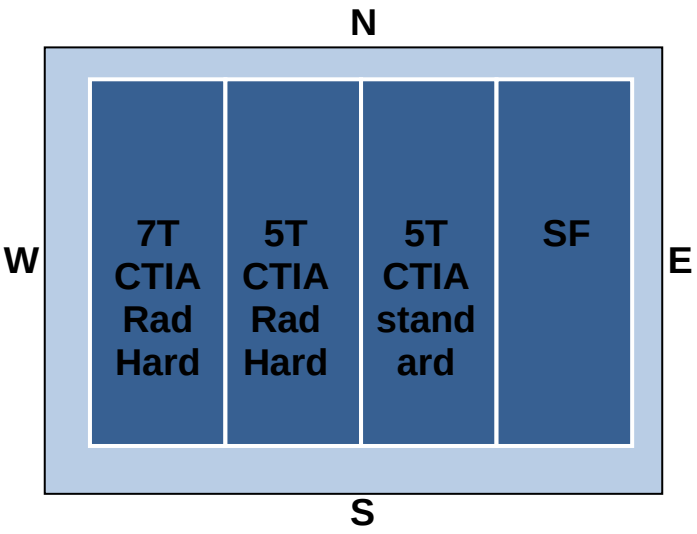

Figure 1: location of the segments containing different input cell topologies.

Although a source follower state was implemented, the targeted solution is based on a CTIA input cell approach. The basic schematic is given in Figure 2. Using this approach the pixel cell topography the capable for the requirements sketched in Table 1.

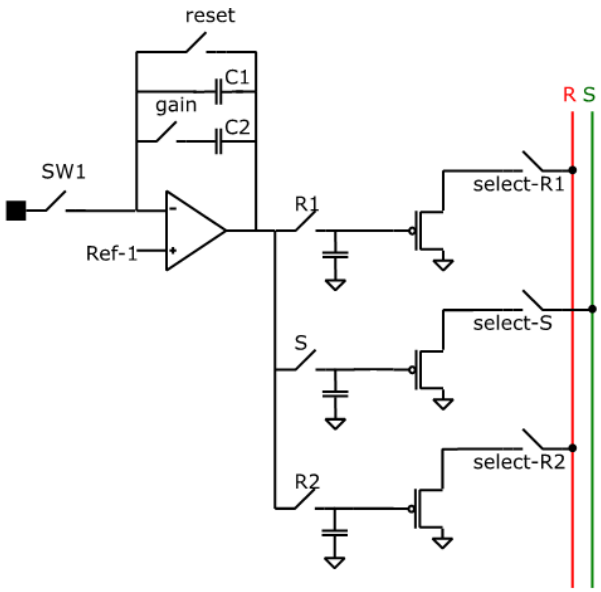

Figure 2: basic topology of a CTIA pixel cell.

In contrary to the regular approach for AIM to include a state machine into the ROIC to control the internal timing, this design is based on a fast serial interface (advanced SPI) ASPI, which is used to address the each of these switches directly by the ASPI data (Figure 3). Toggling of a switch requires uploading logic ‘1’ and logic ‘0’ for a particular ASPI bit. By this approach any shutter mode or special test case can be programmed by an external FPGA through the ASPI interface.

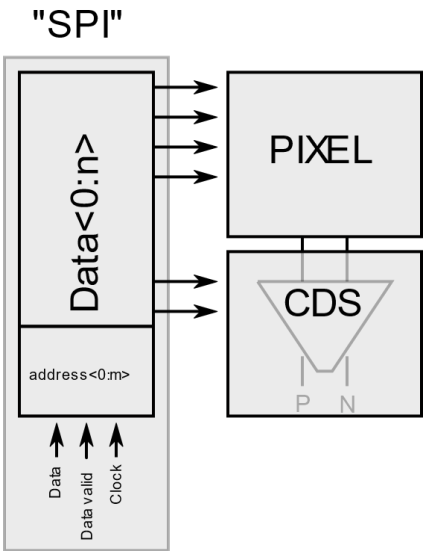

Figure 3: Setup for direct cell control over ASPI bus.

Another implemented feature is the availability of dummy test pixels on the ROIC, implemented as resistive or capacitive loads switched to some pixels on the periphery of the Array. A bias voltage or voltage sweep can be applied to these points to imitate an irradiated photo diode. In Figure 4 a test result using a voltage sweep for the different capacitive coupling is shown, providing an extended characterization capability of the ROIC before hybridization.

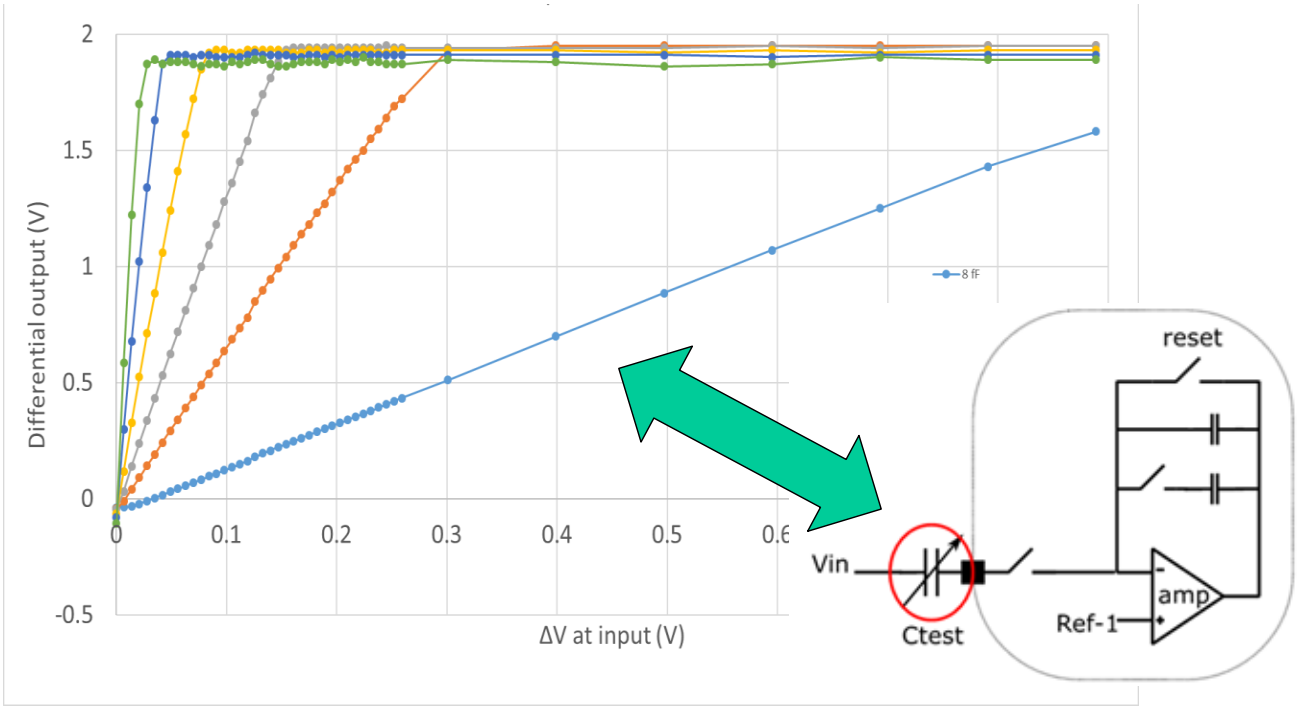

Figure 4: ROIC test result for voltage swing measurement using specific capacitive test structures.

4. TEST CRYOSTAT

For this program a cryostat was set up to allow a measurement of the devices without any residual background. This task was done by the Astronomy group of the Cardiff University. The Figure 5 is outlining the design of this test device. Based on a standard liquid Helium cryostat the thermal and electrical interface was installed to operate the devices between 80K and 30K. Special care was taken to ensure a light tight design and having the flexibility to measure the device alternatively with external sources. Therefore a special shutter was installed having an operational temperature near the LHe temperature.

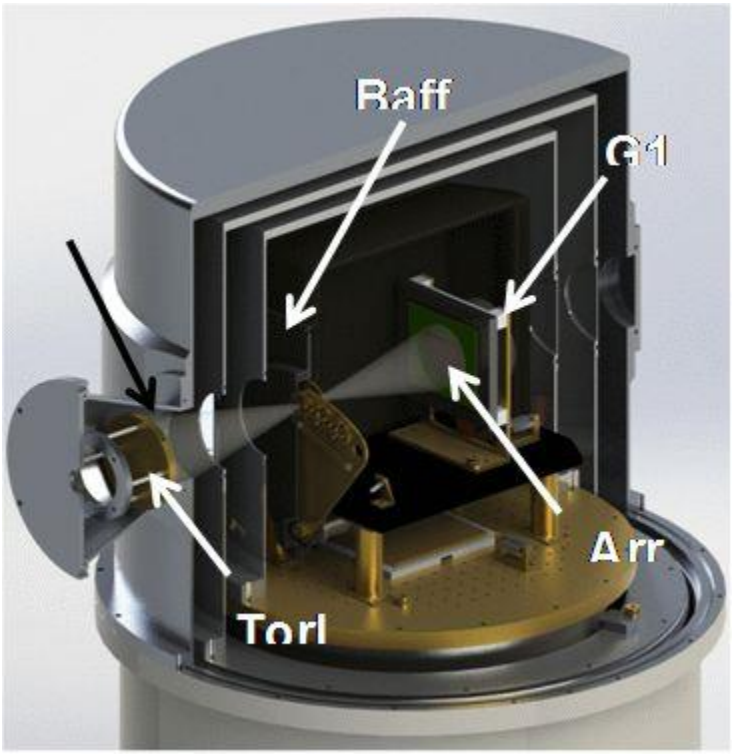

Figure 5: Sketch of cryostat setup.

5. MCT – DEVICES

The MCT devices for this program were processed by AIM as well as the hybridization and assembly into a test housing. The test approach was twofold: a first assembly to get an overview of the performance estimation for the different input stages, on the second step a dedicated test assembly with the best suited MCT/CTIA combination. Therefore small test devices having 320x320 pixel array size were processed to be selectively hybridized onto the different segments.

For the test devices MCT material for n on p and p on n type MCT diodes was processed. For each type two different doping levels were evaluated, so in summary four different MCT devices were available for the testing. Both types of MCT material was designed to have a cut-off wavelength of 12.5 µm at 40K operating temperature.

The material was pre-characterised before hybridization. The reverse bias curves are shown below. For the n on p type the reverse bias characteristic doesn't show any significant differences between the both doping levels. (Figure 6)

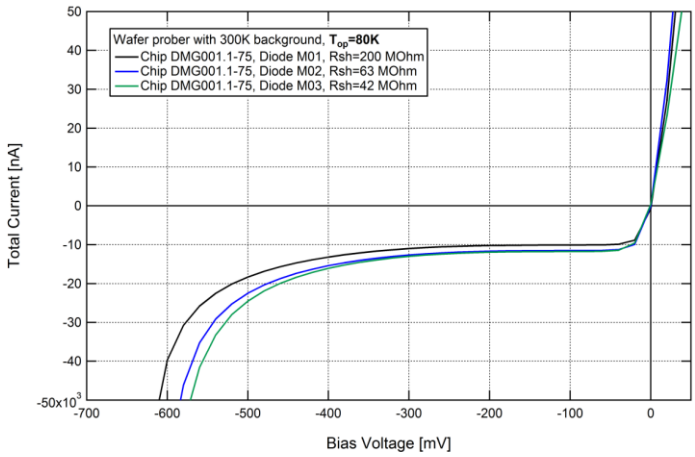

Figure 6: Reverse Bias curves for n on p MCT material (cut-off: 12,5 µm @ 40K).

For the MCT diode type P on N a significant difference in the reverse bias condition was observed. Figure 7 shows an enlarged voltage range having a nearly constant reverse bias current. This is indicating a significant increase of the breakdown voltage of these devices which gives a better possibility to tune the operating conditions of this type of device.

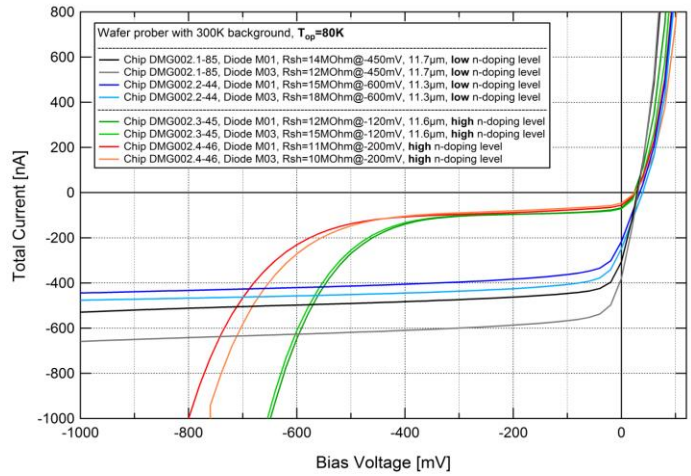

Figure 7: Reverse Bias curves for p on n MCT material (cut-off: 12,6 µm @ 40K).

6. TEST DEVICES

In order to assess the best combination of MCT device and input stage topology a first assembly was done putting Three MCT arrays on one ROIC to assess the performance of the different input stage topologies. This was done for both types of material separately. Figure 8 shows a sample hybrid comprising three MCT chips on a ROIC. The final assembly is shown in Figure 9.

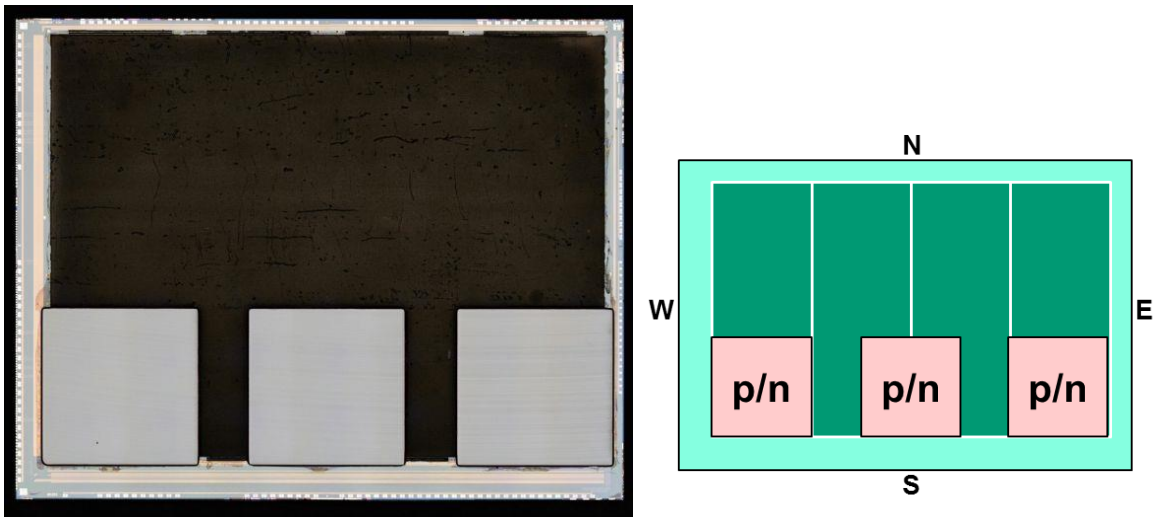

Figure 8: Test hybrid with three MCT chips for initial assessment. Location on the segments is sketched on the right side

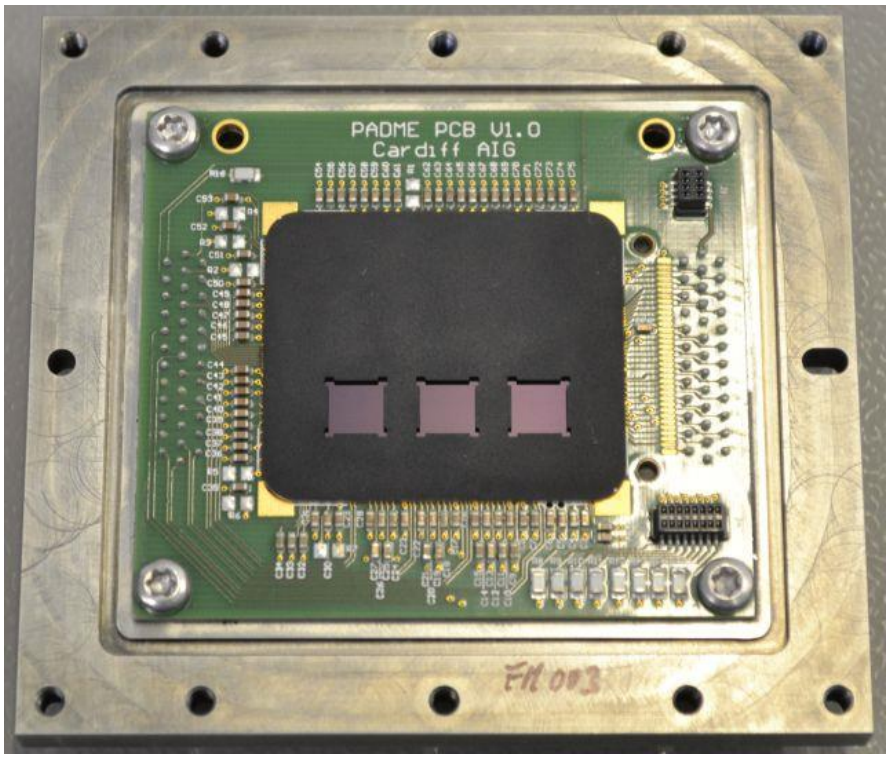

Figure 9: Test detector for initial performance test.

In this configuration especially for 5T input stage topology the two different versions using rad-hard and non-rad-hard ROIC cell library can be directly compared due to the same MCT characteristic on the common chip. The image representation for this special configuration is shown in Figure 10. One part of the MCT array is read out using the rad hard design (left fraction), the other part of the array is read out by the input stage using the standard cell library (right fraction). Both the signal and noise response is given.

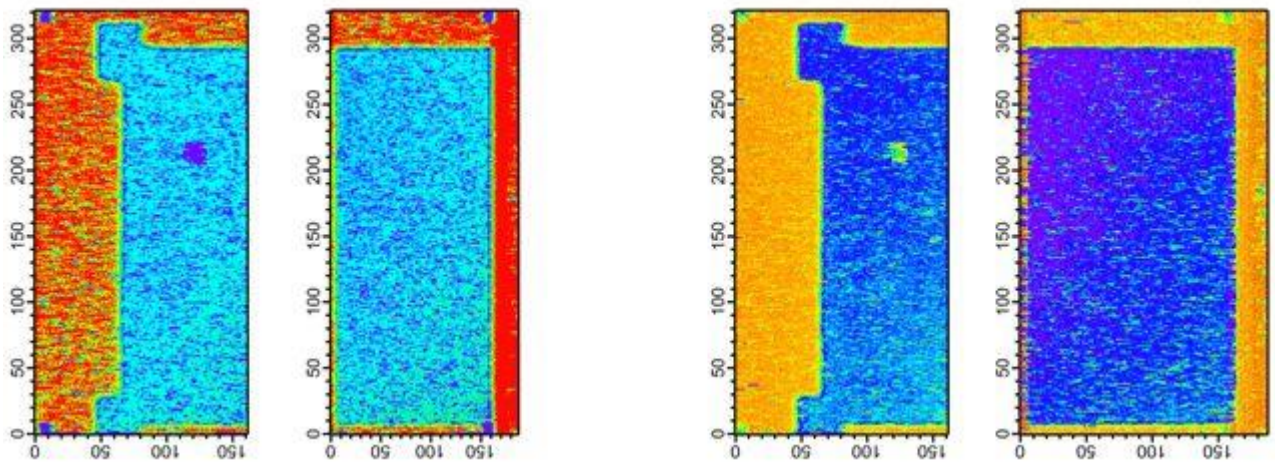

Figure 10: Response of center MCT element: signal response (left) and noise response (right).

Based on this initial assessment two demonstrator devices were assembled with the best suitable combination for input cell topology and MCT material. For the n on p – type MCT devices the 7T input stage topology was selected. For the p on n – type MCT diodes the rad-hard version of the 5T cell was selected for final assembly. In both case MCT devices with different doping levels were used; the device with lower doping level in the upper part of the segment, the device with the higher doping level in the lower part. Figure 11 shows the assembled devices. These parts are subjected to an intensive test campaign to elaborate the characteristic behavior of these detectors. A basic set of test results will be presented on the poster. Among this are the latest test results for the dark currents, which were found significantly decreased already in the pre-test. With this overall test approach the lowest dark currents ever reported for operating temperatures of 40K and below could be measured (Figure 12).

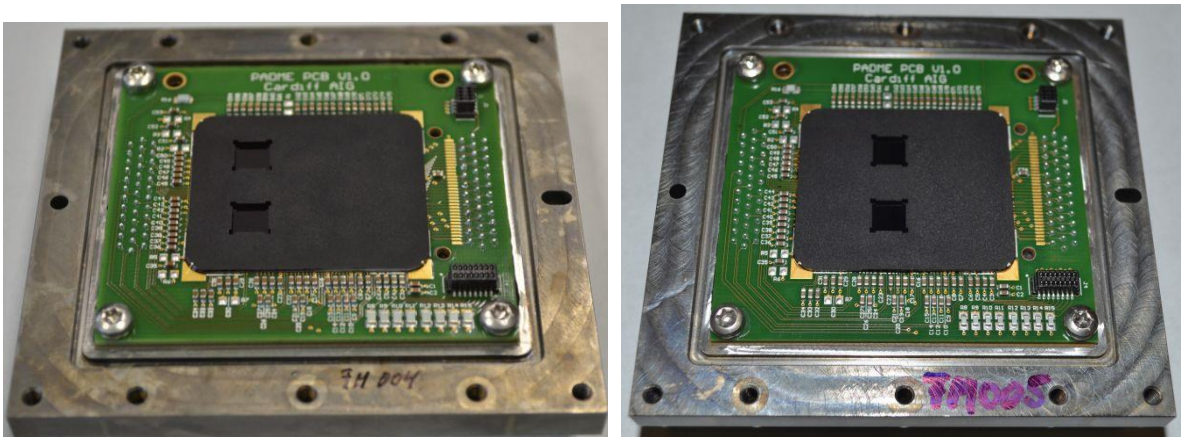

Figure 11: Assemblies of final test devices for n on p type (left) and p on n type (right) Detectors.

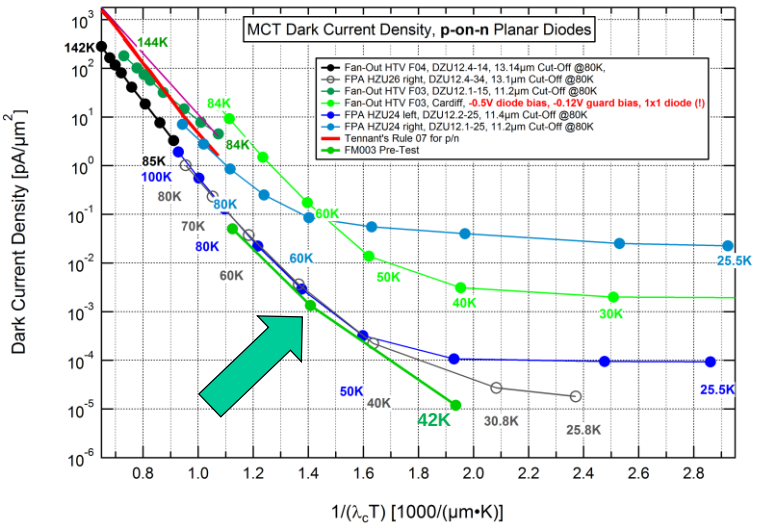

Figure 12: Dark current results from pre-test: dark current result at 42K below all former measurement, no settling found (green curve).

ACKNOWLEDGMENT

This work has been funded by the ESA TRP program “Development of low dark current MWIR/LWIR Detectors”, Ref . 4000113065/15/NL/RA